

Islamic Azad University

Shiraz branch

Faculty of Science, Agriculture, and New Technologies

Thesis for the Award of the Master of Science (MSc) Degree

Title:

Theoretical Study of the Effect of Electron Capture Time on Reducing Threshold Current Density for Performance Improvement of Spin-Polarized Quantum Dot Lasers

Superviser:

Dr. Seyedah Nasrin Hosseini Mutlaq

By:

Abbas Hossein Fazil Al-Ahnaf

Absrtact:

In this research, the mechanism of threshold current density reduction in quantum dot-based semiconductor lasers is examined. Spin injection is utilized as a method for generating spin-polarized carriers, and the rate equations governing these systems are solved numerically. The results indicate that reducing the electron capture time and increasing the polarization of the injected current lead to a decrease in threshold current density and an enhancement in the spin filtering range. The maximum reduction in threshold current density is 0.353, and the normalized spin filtering range is 0.90. Furthermore, the optimal conditions for achieving the maximum spin-up optical efficiency (equivalent to 17.70) are calculated.

Chapter1: Introduction

Semiconductor lasers are of significant importance due to their wide wavelength range, high efficiency, and diverse applications in industries such as telecommunications, medicine, and spectroscopy. These lasers are categorized into two types: dipole (such as quantum dot lasers) and unipolar (such as cascade quantum lasers). Dipole lasers are highly popular due to their high optical efficiency and low temperature sensitivity. In contrast, unipolar lasers have the ability to generate mid- and far-infrared wavelengths, making them particularly useful in fields such as medical imaging and gas detection. This study investigates spin-polarized semiconductor lasers using spinpolarized injection. The main objective is to explore the effects of electron capture time and injection current polarization on the reduction of threshold current density and the spin filtering range. The relevant numerical rate equations are solved, and optimal conditions for achieving maximum optical efficiency are presented. The results demonstrate that spin-polarized injection can contribute to reducing threshold current density and increasing the normalized spin filtering range, thus creating conditions for achieving high optical efficiency. Quantum dots are semiconductor nanocrystals with sizes ranging from 1 to 100 nanometers, whose unique optical and electrical properties can only be explained by quantum mechanics. Their small size leads to the quantization of energy levels and the dependence of emitted light color on dot size; smaller dots emit blue light, while larger dots emit red light. When quantum dots are excited by light, electric fields, or heat, electrons move from the valence band to the conduction band and emit photons upon returning to the ground state. Due to the increased energy gap in quantum dots, this process results in the emission of shorter wavelength and brighter light compared to bulk materials. Quantum confinement occurs when the dot size is smaller than the Bohr exciton radius, altering their optical and electrical properties. III-V quantum dots have high stability due to covalent bonding but exhibit lower quantum efficiency. The tunability of emission wavelength and changes in electrical conductivity of these nanocrystals have led to widespread applications in optoelectronics, medical imaging, and biosensors.

Quantum Dot Lasers:

A quantum dot laser is a semiconductor laser that uses quantum dots as the active medium for light generation. The operation of this laser is based on the pumping of electrons from the valence band to the conduction band of the quantum dots, creating electron holes in the valence band. The recombination of electrons and holes results in the emission of light with energy corresponding to the energy gap and the energy states of the bands. To increase the density of quantum dots, layers of these dots are stacked on top of each other. Semiconductor lasers are of great importance due to their wide applications in technology and industry. By introducing spin-polarized carriers, the threshold current density can be reduced, and the laser efficiency can be improved. Spin-polarized semiconductor lasers, especially Vertical Cavity Surface Emitting Lasers (VCSELs), feature active regions made of III-V quantum dots and use Distributed Bragg Reflectors (DBRs) to create optical resonance cavities. These lasers consume less energy and have a lower threshold current compared to other semiconductor lasers, but their output power is generally lower. This study investigates the effects of spin-polarized injection and electron capture time on reducing the threshold current density and enhancing the normalized spin filtering range. The rate equations governing spin-polarized and non-polarized lasers are solved numerically to determine the optimal conditions for achieving maximum optical efficiency. The results show that spin-polarized injection not only reduces the threshold current density but also improves the spin filtering range, thereby enhancing the optical efficiency of the laser.

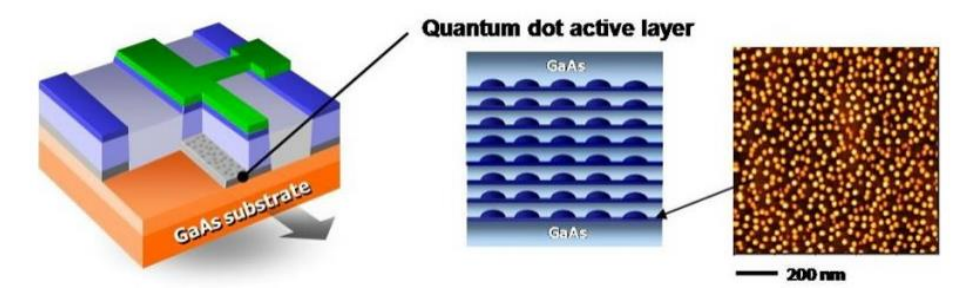


Figure 1: A quantum dot laser showing an active layer containing rows of high-density quantum dots.

Materials for Spin-Polarized Injection:

Spin-polarized electron injection into semiconductors is used in spintronics. This current is generated from ferromagnetic materials due to the difference in the density of states for high and low spin electrons. To achieve spin-polarized injection, ferromagnetic materials with high Curie temperature and fast switching times are typically used; however, a challenge arises due to the mismatch in conductivity between the ferromagnetic materials and the semiconductors. Solutions to this issue include the use of half-metallic ferromagnets, dilute magnetic semiconductors, or external tunneling barriers. In this study, the effects of electron capture time and injection current polarization on reducing threshold current density and enhancing the normalized spin filtering range in spin-polarized semiconductor lasers are investigated by solving the numerical rate equations.

Chapter 2: Fundamentals of Spintronics and Spintronic Lasers

Spintronics, or spin-electronics, is the study of electron spin and the associated magnetic moment. Unlike electronics, which focuses solely on the electron's electric charge, spintronics also considers the additional degree of freedom of the electron's spin (either up or down). Controlling this spin state is a complex task; however, recent advances have been made in understanding and manipulating it. Spintronics is still in its early stages, with the first spintronic devices being

discovered and developed in the 1990s. This field has the potential to lead to significant advancements in information storage and transmission, increase the speed of data storage, and improve performance in future technologies. This report introduces the fundamentals of spintronics and explores its applications in industry and research.

Electron Spin:

Materials are composed of atoms, which include a nucleus and electrons. In solids, electrons can occupy different energy levels, which determine the physical properties of the material. Specifically, electrons are the primary contributors to the magnetic properties of materials. In ferromagnetic materials, the electron spins align in a coordinated manner, generating a magnetic field, while in non-magnetic materials, the spins are arranged randomly, neutralizing the magnetic field. Spin polarization refers to the ratio of up-spin to down-spin electrons, which determines the magnetic characteristics of a material. Ferromagnetic materials such as iron and cobalt exhibit higher spin polarization.

Out-of-Equilibrium Spin or Polarization:

At room temperature and under normal conditions, the number of up-spin and down-spin electrons in a material reaches equilibrium, which determines its magnetic state without the application of external force or field. This equilibrium can be disturbed by the injection or pumping of electron spins, creating a polarized or out-of-equilibrium spin state. When the injection stops, the spins return to their equilibrium state. The time required for the spins to return to equilibrium is referred to as the spin relaxation time. This spin injection can occur through conductive, optical, or resonant methods.

Magnetic Multilayers and Their Interesting Properties:

Ferromagnetism and paramagnetism are two major types of magnetic materials, and their sequential coupling results in interesting electrical properties. These properties contributed to the formation of the field of spintronics. The coupling of two magnetic materials can create direct magnetic effects at their interface, known as magnetic coupling. Placing a non-magnetic material between two ferromagnetic materials can enhance this coupling, and the thickness of the non-magnetic layer influences the type of coupling. The coupling can be ferromagnetic or antiferromagnetic, meaning the ferromagnetic layers can align either parallel or antiparallel to each other. For instance, in a three-layer structure with cobalt (ferromagnetic) and copper (non-magnetic) layers, changing the thickness of the copper layer can alter the coupling type from antiferromagnetic to ferromagnetic and vice versa.

Giant Magnetoresistance (GMR):

Magnetoresistance (MR) is a measure of the change in electrical resistance due to the application of an external magnetic field. Materials with higher magnetoresistance are more sensitive to magnetic fields, and greater changes in resistance are observed when a magnetic field is applied. In structures with antiferromagnetic coupling, the electric current passing through exhibits higher resistance compared to structures with ferromagnetic coupling. It is possible to align the magnetic orientation of the layers by applying a magnetic field, creating a material whose electrical

resistance changes. This phenomenon is known as Giant Magnetoresistance (GMR) and can be used in the development of sensors sensitive to external magnetic fields. In such structures, when an external magnetic field is applied, the magnetic orientations of the layers align, and the resistance decreases. This phenomenon arises due to the misalignment of electron spins in different environments, which disrupts electron motion and increases electrical resistance.

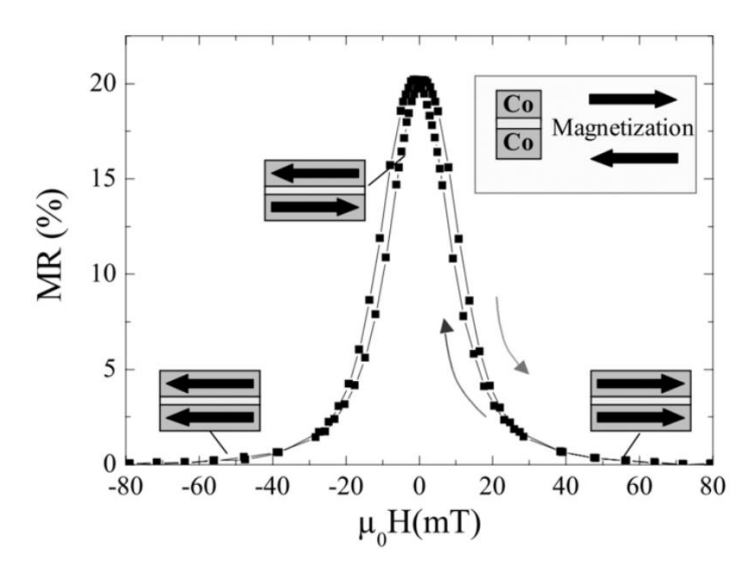


Figure 2: Measured MR curve of Co/Cu layers, showing the dependence of the GMR effect and the magnetic orientation of these layers on the external magnetic field.

Tunnel Magnetoresistance (TMR):

In Giant Magnetoresistance (GMR), it is assumed that the intermediate layer is a non-magnetic conductor or semiconductor, allowing electrons to pass through it easily. However, if the intermediate layer is insulating, such as oxide layers, electrons require a phenomenon called electron tunneling to pass through this layer. This phenomenon is observed in structures known as Tunnel Magnetoresistance (TMR). In TMR, electron tunneling only occurs when the electron spins in both ferromagnetic layers are aligned. This results in TMR structures providing a greater barrier to electron flow, showing significantly higher electrical resistance under antiferromagnetic coupling conditions compared to GMR. In practice, the magnetoresistance in TMR structures is substantially higher than in GMR, a feature that enhances the sensitivity of sensors.

Applications of Spintronics:

1) GMR-based Devices:

In various GMR structures, electric current passes through ferromagnetic and non-magnetic layers, and the electrical resistance changes depending on the orientation of the magnetic moments of the layers. In different models, resistance changes arise from the magnetic interactions between the layers and the type of couplings. In FM/NM structures, the current can flow either in-plane or perpendicular to the plane, and here, the orientation of the magnetic moments of the layers results in the GMR effect. In the SoftFM/NM/HardFM three-layer model, soft magnetic layers change direction in small magnetic fields, while hard magnetic layers maintain their orientation, and these

changes give rise to the GMR effect. The spin-valve model, utilizing ferromagnetic and antiferromagnetic layers, locks the magnetization direction, and the GMR effect occurs due to the misalignment of the magnetizations. These models are used in sensor technologies and other magnetic applications for measuring changes in electrical resistance and sensitivity to magnetic fields.

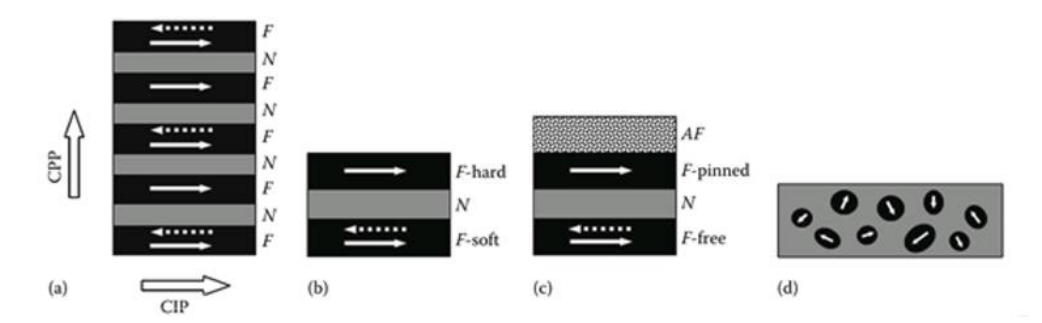


Figure 3: Types of GMR structures. a) Multilayer GMR, b) GMR based on the hardness and softness of magnetic layers, c) Spin-valve GMR, and d) Composite GMR.

2) Hard Disk Drive (HDD) Read-Head:

The read-heads, which are essentially magnetic sensors based on GMR structures, are small components of hard disk drives that are positioned over the spinning disk surface. These read-heads detect the information stored on the hard disk in the form of magnetic bits (high or low magnetization). As the hard disk spins beneath the read-head, these bits are read by the GMR sensors and translated into binary values (0 or 1). In 1998, the development of GMR-based read-heads revolutionized the data storage industry, as these sensors enabled the detection of smaller bits and significantly increased storage capacity. This achievement marked the first industrial application of spintronics, drawing significant attention to the field.

Spintronic Devices Based on TMR:

1) MTJs (Magnetic Tunnel Junctions):

MTJs (Magnetic Tunnel Junctions) are spintronic devices based on the TMR (Tunnel Magnetoresistance) phenomenon. These devices typically consist of non-magnetic insulating layers made of materials like aluminum oxide (Al₂O₃) or magnesium oxide (MgO), sandwiched between two ferromagnetic layers. Extensive research has been conducted in this field, and scientists have successfully created MTJs with high magnetoresistance by adjusting the thickness of the magnetic and non-magnetic layers. The fabrication and control of these devices require very precise and sensitive techniques, along with advanced, expensive equipment. As a result, only a limited number of academic institutions have the resources and expertise to conduct research and scientific work in this area.

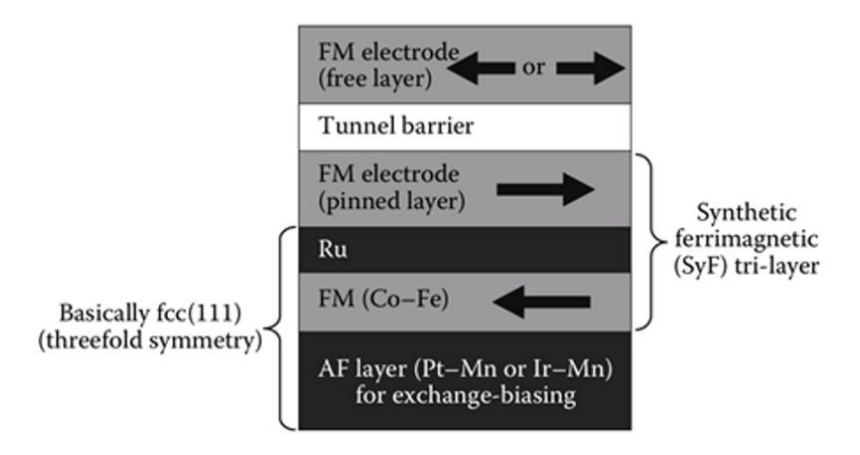


Figure 4: A schematic of the cross-sectional structure of an MTJ device.

2) Spin Oscillators:

Magnesium oxide (MgO)-based MTJs have a high potential for microwave applications. When an alternating current with microwave frequency passes through an MTJ structure, a DC voltage is generated across it. As a result, MgO-based MTJs can function as microwave wave sensors. These spin oscillators, known as STNOs (Spin-Torque Nano-Oscillators), offer superior features compared to conventional types. Notably, their state can be tuned by a bias current or an external magnetic field, they are significantly smaller in size, and they can operate across a wider temperature range.

Magnetic Sensors:

GMR and TMR devices, as magnetic sensors, are capable of detecting magnetic fields. All objects generate magnetic fields, including humans, whose hearts produce magnetic pulses in the picotesla range, revealing important cardiac information. Additionally, rotating disks inside hard drives emit magnetic signals. The Earth's magnetic field can also serve as a navigation tool in areas where GPS systems are unavailable. Highly sensitive magnetic sensors are used in various industrial and consumer applications. In magnetocardiography (MCG), these sensors are used to measure the weak electrical signals emitted by the beating heart, helping to assess heart function. Similarly, in magnetoencephalography (MEG), magnetic sensors are employed to measure electrical activity in the brain, which can assist in identifying problematic brain areas and aid in brain surgeries. Although SQUIDs (Superconducting Quantum Interference Devices) are used in these fields due to their high sensitivity, these devices are expensive and require very low temperatures to function.

Magnetic RAM (MRAM):

MRAM (Magnetic Random Access Memory) is a type of memory that stores information permanently and does not require a constant power supply, unlike traditional RAM, where data is lost when power is turned off. MRAM utilizes magnetic states to represent data bits, which can be read by an electrical current. Because of its unique features, MRAM can significantly enhance the speed and accuracy of information processing in computers and electronic devices. As a promising application of spintronics, MRAM is capable of providing non-volatile storage without the need for continuous energy, making it an attractive option for future memory technologies.

Schottky Diode:

In a regular p-n diode, p-type and n-type semiconductors are joined to form a p-n junction. However, in a Schottky diode, metals such as aluminum or platinum replace the p-type semiconductor. This diode is named after the German physicist Walter Schottky and is commonly used in radio frequency (RF) applications. In a Schottky diode, when a metal contacts an n-type semiconductor, a metal-semiconductor (M-S) junction is formed, creating a Schottky barrier. This diode switches on and off much faster than a traditional p-n junction diode and produces less unwanted noise, making it very useful in high-speed switching circuits. The voltage required to turn on a Schottky diode is between 0.2 to 0.3 volts, which is lower than that of silicon diodes (0.6 to 0.7 volts). This behavior is similar to germanium diodes, but Schottky diodes are preferred over germanium due to their faster switching speeds.

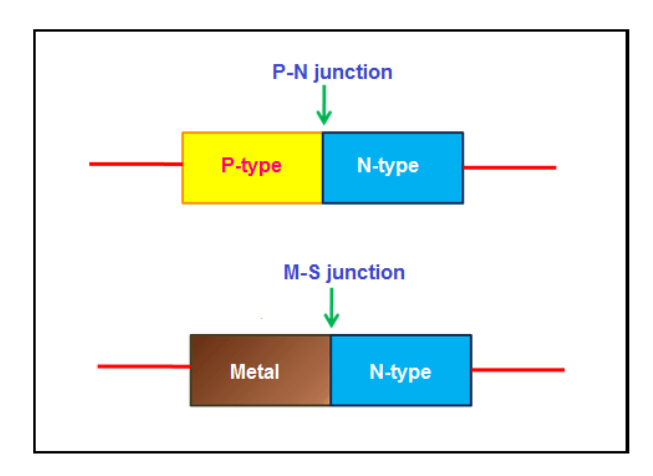


Figure 5: Illustration of P-N and M-S junctions.

Schottky Barrier:

In a Schottky barrier, a depletion region forms at the interface between the metal and the n-type semiconductor. This Schottky barrier acts as a potential energy barrier that controls the flow of electrons. When a metal contacts an n-type semiconductor, this metal-semiconductor junction forms a rectifying or non-rectifying Schottky barrier. A rectifying Schottky barrier (also called a one-way barrier) is formed when the contact is made with a moderately doped semiconductor, and it creates higher resistance to electrical current compared to ohmic contacts. On the other hand, a non-rectifying barrier is formed when the contact is made with a highly doped semiconductor, resulting in lower resistance. The height of the Schottky barrier depends on the composition of the semiconductor and metal. In the case of a non-rectifying barrier, the barrier height is low enough that the depletion region does not form. In contrast, for a rectifying barrier, the barrier is large enough to create a depletion region. For the construction of a Schottky diode, when a metal contacts an n-type semiconductor, the energy level of the semiconductor electrons is higher than that of the metal electrons. This energy difference, known as the built-in voltage (Vbi) of the Schottky diode, represents the difference in electron extraction energy between the semiconductor and the metal. As a result, Schottky diodes can switch on and off faster than traditional diodes,

making them highly efficient in high-frequency switching circuits. The energy band diagram of the semiconductor and metal after contact also illustrates this energy difference.

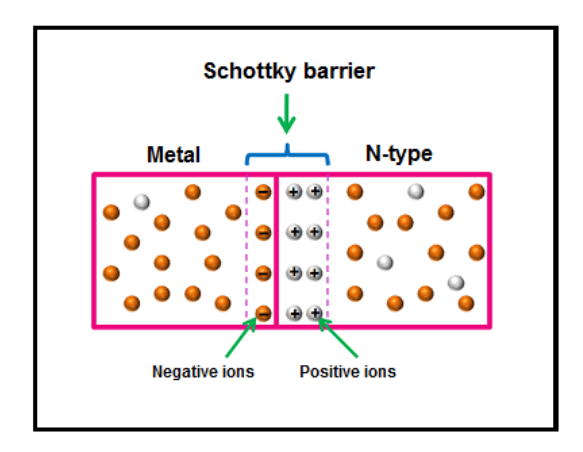


Figure 6: Schottky barrier

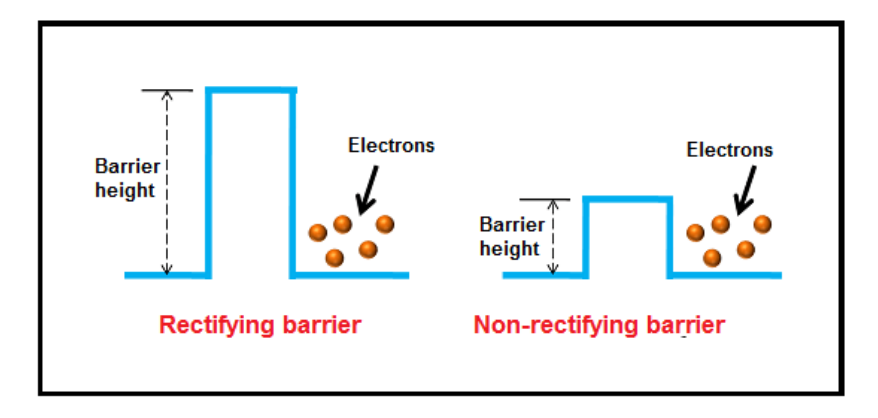


Figure 7: Rectifying and non-rectifying Schottky barriers

Analytical Review of Spin-Polarized Semiconductor Lasers:

Spin-polarized semiconductor lasers are one of the most significant outcomes of research in spintronics, and their theoretical description is complex. These lasers typically operate as vertical-cavity surface-emitting lasers (VCSELs). In these lasers, spin injection through electrical means reduces the threshold current density and enhances dynamic performance. A lower threshold current density leads to reduced energy consumption and increased efficiency of the lasers. Compared to traditional lasers, where carriers have unpolarized spins, spin-polarized semiconductor lasers exhibit different behavior due to the influence of spin polarization on the emitted light. These lasers can be categorized based on the injection of spin-polarized or unpolarized carriers. In spin-polarized lasers, the emitted light is affected by the spin polarization of the carriers, meaning the emission exhibits circular polarization. The structure of these lasers includes an active region, a resonant cavity, and a carrier injector. The light emission process occurs through the recombination of electrons and holes. The threshold current, which determines when the laser will start emitting light, must be precisely controlled for optimal performance. In spin-polarized semiconductor lasers, spin injection can be achieved with two ferromagnetic

contacts. These lasers, due to the presence of left- and right-handed circular polarization, exhibit two distinct laser emission modes with unequal intensities. Additionally, there are significant differences between quantum well (QW)-based lasers and quantum dot (QD)-based lasers. QD-based lasers involve more complex mechanisms, including the wetting layer acting as a carrier reservoir. These lasers are influenced by the Pauli exclusion principle and saturation of wetting layer states, which are especially relevant in the injection of spin-polarized carriers. In conclusion, spin-polarized semiconductor lasers are capable of controlling the emitted light precisely through spin injection, providing unique performance characteristics, such as circular polarization, which are not observed in conventional lasers.

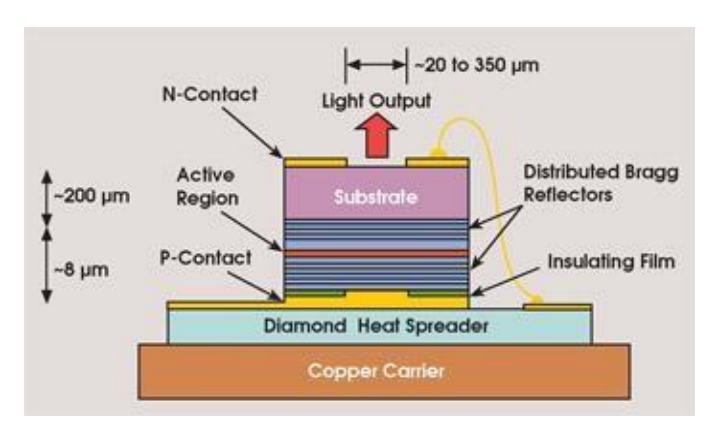


Figure 8: Vertical-Cavity Surface-Emitting Laser (VCSEL).

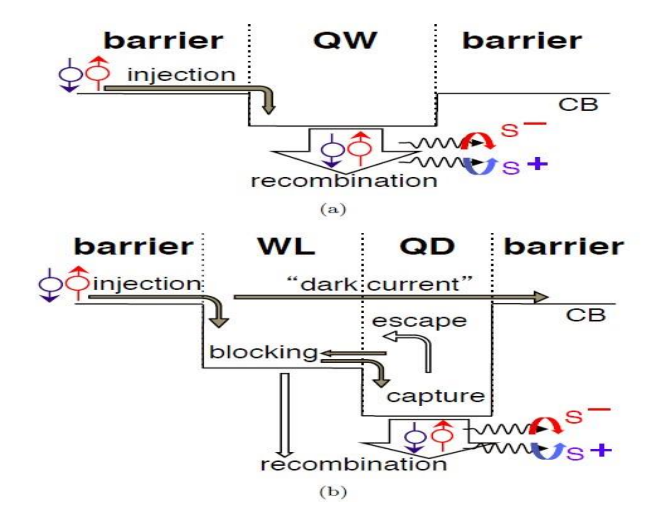


Figure 9: Energy band diagram of a semiconductor laser and carrier injection steps(a) Quantum Well (QW) laser: A spin alignment between injected carriers leads to the recombination of some electron-hole pairs, resulting in circularly polarized emitted light. The emitted photons with positive and negative helicity are denoted as (b) Quantum Dot (QD) laser: It includes an additional energy level due to the wetting layer (WL), and several additional stages that are not present in Quantum Well lasers..

Bucket Model for Spin-Polarized Lasers:

The bucket model is a conceptual framework used to describe the behavior of spin-polarized semiconductor lasers, visualizing their operation through an analogy to a water system. In this analogy, the water level represents the carrier density, and the water faucet represents the spinpolarized carrier injection. The output water signifies the emitted light intensity, and the small holes represent the spontaneous recombination processes within the system. In the case of low injection, the water level is low, and only weak light is emitted, similar to conventional lasers that rely on spontaneous and instantaneous recombination. As the injection increases, the water level approaches the laser threshold, and the emitted light intensity increases significantly. At the injection threshold J_T the spontaneous emission begins, and the intensity of light rises dramatically. When the injection current exceeds the threshold $(J > J_T)$ the process of stimulated recombination becomes dominant. The bucket model also involves a comparison between two spin populations, which are metaphorically divided into cold and warm water. This division specifically addresses the effects of spin polarization. If the boundary between these two populations (cold and warm water) is small, the spins do not mix, which corresponds to the idea of an unlimited spin polarization. However, if the boundary is large, the populations quickly reach equilibrium, leading to the loss of the spin polarization of the carriers. This behavior represents the complexities of spin-polarized carrier injection and its impact on the performance of spin-polarized semiconductor lasers. In this model, with unequal injection of cold and warm water, the spin polarization of the injected carriers is defined, and the behavior of the system can be analyzed in terms of how spinpolarization affects the laser's output. The system's dynamics depend on how effectively spinpolarized carriers are injected and how they interact with each other within the device. This model provides an intuitive way to understand the intricacies of spin-polarized carrier injection and the resulting effects on the laser's performance, shedding light on the role of spin-polarization in semiconductor laser behavior.

$$P_{J} = (J_{+} - J_{-})/J \tag{1}$$

In this, J_{\pm} refers to the injection of two spin states that together constitute the total injection (electric-spin injection): $J=J_+-J_-$ and Δ represents the difference between the cold and warm water levels, leading to three operational regions for the carriers and two distinct lasing thresholds, $J_{T1,2}$. Small holes indicate carrier loss through spontaneous recombination. The total electron density is written as $n=n_++n_-$ the total hole density as $p=p_++p_-$, and the total photon density as $s=s_++s_-$ When the spin population is zero, it is expected that spin-polarized and non-polarized semiconductor lasers will behave similarly. According to the Bucket model, the performance of spin-polarized lasers is intuitively understandable. With two unequal carrier populations (majority and minority spins), there are two distinct lasing thresholds. The half of the bucket that fills faster will overflow first, indicating that lasing (resonance) occurs initially due to majority spin carriers. When the other half is sufficiently filled, lasing for minority spin carriers is expected. Based on the Bucket model, spin-polarized lasers have two threshold current densities, $J_{T1,2}$ which correspond to the majority and minority spin carriers, respectively. These lasers have three operational regions:

Region I: Where there is no stimulated emission, and the laser is in the "off" state.

Region II: Where majority spin carriers cause lasing. This region is known as the normalized spin-filtering range.

Region III: Where both spin carriers contribute to lasing.

At low pumping (when the cold and hot water levels are below threshold), both high-spin and low-spin carriers are in the "off" region (LED), and the light emission is minimal. At higher pumping, the hot water level reaches the threshold and overflows, while the cold water level is still low and only slightly overflows. This stage represents the region where majority spin carriers reach lasing, while minority spin carriers are still in the LED region. In this case, the induced emission is due to recombination of majority spin carriers. Key results from this model, confirmed by experiments, are that spin lasers start lasing at a lower threshold compared to conventional lasers, as only part of the bucket needs to be filled. This indicates a reduced threshold for spin lasers. These parameters can be written as follows:

$$r = \eta - \frac{J_{T2}}{J_T} \tag{2}$$

where J_{T2} is the majority spin threshold $J_{T1} < J_T$

2) Even a moderate spin polarization, $P_J \le 1$ can result in significantly high circularly polarized light. The relative width of the "spin-filtered region" can be expressed in terms of the distance as follows:

$$d = {(J_{T1} - J_{T2})}/{J_T} (3)$$

Where J_{T2} is the minority spin threshold $J_{T1} \le J_T \le J_{T2}$, and the width of this range increases with spin polarization injection. For $J > J_{T2}$ the helicity of the minority spin photon carriers decreases, and the spin polarization of the light converges to $-P_I$ as the injection increases.

Chapter 3: An Overview of Nanotechnology

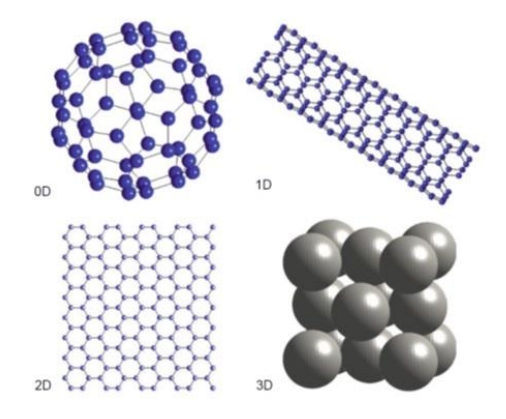
Nanotechnology involves making changes and optimizations at scales ranging from 1 to 100 nanometers and is particularly significant due to the unique properties of materials at these small scales. Nanoparticles at the nanoscale exhibit properties that are vastly different from those of materials at conventional sizes. These differences arise from the distinct interactions at the nanoscale, where classical physics laws can no longer explain the behavior, requiring the use of quantum mechanics for their interpretation. For example, gold nanoparticles have different chemical and physical properties and can be liquid and easily reactive, whereas gold at conventional sizes is solid. Copper nanoparticles can be transparent, aluminum nanoparticles can easily burn, and silicon nanoparticles, unlike bulk silicon, are conductive. These changes in material behavior at the nanoscale have led to extensive applications in various scientific fields such as medicine, electronics, energy, and new materials.

Methods for Fabricating Nanodevices:

In nanotechnology, there are two main approaches for fabricating devices: the "top-down" method and the "bottom-up" method. In the top-down method, similar to making a chair from a tree trunk, larger pieces are first divided into nanoscale sizes. This method is used for fabricating microprocessors in the computer industry, but it is inefficient when atomic-scale alterations are required, as it does not allow control over the arrangement of atoms. Another issue with this method is the roughness of the product's surface. The bottom-up method, where pieces are assembled by the joining of atoms, is more akin to natural processes. This method, by accurately simulating chemical, physical, and biological processes in the laboratory, can create precise and carefully designed structures. One interesting example of this approach is "self-assembly," where molecules automatically form an orderly structure on a surface. Unlike the top-down method, this approach allows for the creation of such structures. The use of the bottom-up method for designing and fabricating materials and processes represents a revolution not only in terms of technological complexity but also in the type of thinking involved. The properties of atoms in these structures directly influence the microscopic properties and even the physical appearance of the products. Additionally, this method can contribute to the production of products with high biocompatibility and minimal environmental impact. Researchers hope that by drawing inspiration from nature, they will be able to produce environmentally friendly and low-risk products for human societies.

Nanomaterials:

Nanomaterials are categorized into different types, each with specific properties and applications. Zero-dimensional (0D) nanomaterials include nanoparticles, which have less than 100 nanometers in all dimensions and are used in various fields such as electronics, cosmetics, and sports equipment. A well-known example in this group is C60. One-dimensional (1D) nanomaterials include nanowires and nanofibers, which are larger than 100 nanometers in one dimension, and due to their unique mechanical and electrical properties, they are used in different industries. Carbon nanotubes (CNTs) also fall under this category, with their electrical and optical properties depending on the tube diameter and atomic structure. Graphene, a layer of carbon atoms with a unique structure, exhibits remarkable optical and electrical properties. Additionally, structures such as porous anodic alumina (PAA) are used for the storage of materials and specific processes. Ultimately, combining 0D, 1D, and 2D nanoparticles can create three-dimensional structures with interesting features and unique applications.



Applications of Nanotechnology:

Nanotechnology is currently making a significant impact across various industries and will soon transition from a competitive advantage to a fundamental requirement for the production of more efficient products. In the electronics industry, nano transistors with dimensions smaller than 100 nanometers have led to the development of electronic components with lower energy consumption and higher efficiency. In agriculture, nanotechnology has contributed to increased crop yield while using fewer raw materials. In medicine, nanotechnology has led to the development of tools such as nanobots and nanochips for treatment, diagnosis, and tissue regeneration. Furthermore, targeted drug delivery using smart nanoparticles can reduce side effects of medications and enable more precise treatments. In the energy sector, nanotechnology is applied to optimize solar cells and convert sunlight into clean energy. This technology is also used in the military industry for the creation of smart sensors and explosive-resistant materials. In manufacturing, nanomaterials can enhance products by providing properties such as lightweight and higher efficiency. Additionally, by replacing silicon with graphene in the fabrication of silicon components, it is possible to reduce greenhouse gas emissions. These advancements demonstrate that nanotechnology will have a promising future in improving the quality of life and the environment.

Introduction to Quantum Dots:

Quantum dots are semiconductor nanoparticles with dimensions ranging from 1 to 10 nanometers, composed of 200 to 10,000 atoms, and function as semiconductor crystals. These nanostructures are typically made in a core-shell configuration, where the core is composed of elements from groups II-VI or III-V, and is covered with a shell of semiconductor materials. These structures exhibit unique optical and electrical properties due to a phenomenon known as quantum confinement. In this effect, as the size of the nanoparticles decreases, the energy of the band gap (forbidden band) increases, requiring more energy to excite the particles. Quantum dots are used in various applications such as light-emitting diodes (LEDs), lasers, bioimaging, and solar cells. These nanoparticles can emit different colors in the visible spectrum, depending on their size. The smaller the quantum dots, the larger the band gap, resulting in the emission of light with shorter wavelengths (bluer colors).



Figure 11: Image of quantum dots with different colors (due to their varying size and chemical composition).

Optical Properties of Quantum Dots:

Quantum dots exhibit unique electrical and optical properties due to the quantum confinement effect at the nanoscale, distinguishing them from other materials such as organic dyes and fluorophores. This effect arises when the size of the nanoparticles decreases below a critical size or Bohr radius, leading to an increase in the band gap energy and altering their optical properties. One of the main advantages of quantum dots is their broad excitation spectrum, which allows them to be excited by different wavelengths. Unlike organic dyes, which are only excited by a specific wavelength, quantum dots can emit a range of colors from a single excitation wavelength, as their emission spectrum can be tuned over a wide range of wavelengths (from ultraviolet to infrared) by controlling the size and composition of the nanoparticle. Additionally, quantum dots, unlike organic fluorophores that have poor stability under light irradiation, are highly stable and can remain under light exposure for longer periods. This stability allows their fluorescence signal to be detected for extended periods, even after background signals from tissues have decayed. Therefore, the use of quantum dots in medical and biological imaging offers several advantages over other fluorophores, as they can detect specific fluorescence signals without interference from background signals. Alongside their optical properties, quantum dots also possess electrochemical characteristics. When in contact with an electrode surface, they can exhibit photoelectrochemical properties. Under light exposure, these dots can transfer electrons from the valence band to the conduction band, creating electron-hole pairs. This process can lead to the generation of electric current, which has applications in sensors and nanoelectronics.

Synthesis of Quantum Dots and Their Surface Chemistry:

The photochemical and photophysical properties of quantum dots are influenced by factors such as the shell material, core material, and the surface coating. The shells play a critical role in stabilizing these dots, and minor changes in their chemical composition can have significant effects on their optical properties. Quantum dots without shells and surface coatings do not perform optimally because bare cores can develop structural defects over time, leading to phenomena such as blinking. Moreover, the high surface-to-volume ratio of the cores makes them highly reactive and unstable. To enhance the stability and performance of quantum dots, coatings such as zinc sulfide (ZnS) are commonly used, which improve their stability against light exposure and enhance their luminescence. However, coating alone is not sufficient, and to improve compatibility with biological environments, quantum dots should be coated with materials such as polyethylene glycol (PEG). Another important challenge is the solubility of quantum dots in aqueous solvents, which can be improved by modifying their surface chemistry to enhance their solubility in aqueous environments.

Toxicity of Quantum Dots:

Quantum dots can exhibit toxicity and cause cell death or disruption of cellular function. The degree of toxicity depends on factors such as size, concentration, surface chemistry, core composition, and surface coating materials. Three main mechanisms have been proposed for the toxicity of quantum dots on cells: the release of cadmium from the core of the quantum dots, the production of reactive oxygen species (ROS), and interactions with intracellular components.

Quantum dots with cores made from elements in groups III-V, such as gallium arsenide (GaAs), are more stable and exhibit lower toxicity, as the covalent bonds in these dots are more stable compared to the ionic bonds in quantum dots from groups II-VI, such as cadmium selenide (CdSe) and cadmium telluride (CdTe). However, the synthesis of III-V group quantum dots is more complex and time-consuming, and their performance is generally lower than that of II-VI group quantum dots.

Applications of Quantum Dots:

1) Biological Applications:

The use of quantum dots in imaging and the analysis of biological compounds has led to significant advancements in science. These dots, due to their higher brightness and greater stability compared to organic dyes, have numerous applications. Quantum dots are up to 20 times brighter and 100 times more stable than organic dyes. One of their primary applications is in cell or molecular tracking, where quantum dots bind to cells or molecules and cause them to emit light. This feature is beneficial for detecting cancer tumors. However, ultraviolet radiation can increase the toxicity of these dots, especially for quantum dots made from cadmium selenide. This toxicity arises from the release of cadmium ions in the cellular environment. Solutions such as polymer coating of quantum dots and preventing UV exposure have been developed to reduce their toxicity.

2) Photocatalytic Applications:

In recent years, photocatalysts have been developed as environmentally friendly methods for synthesizing organic materials. These catalysts absorb light and activate electron-hole pairs that can react with surface molecules. The use of carbon quantum dots in photocatalysts enables the conversion of visible light into shorter wavelengths, facilitating the excitation of TiO2 to form electron-hole pairs. The combination of carbon quantum dots with TiO2 enhances electron transfer and increases the stability of photocatalytic properties.

Chapter Four: Analytical Study of the Effect of Electron Capture Time on the Reduction of Threshold Current Density in Spin-Polarized Quantum Dot Lasers

Lasers, particularly semiconductor lasers, are of great importance due to their wide practical applications. These lasers use semiconductors as the active medium, where light is amplified through stimulated emission by pumping the active material. Spin-polarized semiconductor lasers, which utilize spin-polarized carriers, can reduce the threshold current density. Vertical cavity surface-emitting lasers (VCSELs) are a type of semiconductor laser where the laser radiation is emitted perpendicular to the surface, using two Bragg distributed reflectors to enhance the light. These lasers are known for their low energy consumption and low threshold current, although they typically have lower output power compared to other lasers. In this study, the impact of electron capture time and the polarization of the injected current on reducing the threshold current density and the normalized spin-filtering range in spin-polarized quantum dot semiconductor lasers is investigated. By solving the numerical rate equations, the effects of electron polarization and electron capture time on these parameters are calculated. Additionally, the high-spin optical gain is calculated, and the conditions for achieving optimal optical gain are analyzed.

Materials for Spin-Polarized Injection:

Spin-polarized electron injection into semiconductors plays a significant role in spintronics. To create this injection, an electron current passes through ferromagnetic materials that act as spin injectors. However, the main problem is the mismatch in conductivity between the ferromagnetic materials and the semiconductors. There are three solutions to this issue: 1) using semimetallic ferromagnets that create full spin polarization, 2) using dilute magnetic semiconductors with conductivity similar to that of ferromagnetic materials, and 3) using a tunneling barrier that allows ferromagnetic materials to serve as a source of spin-polarized electrons.

Rate Equations:

In spin-polarized quantum dot semiconductor lasers, three main processes govern the electron transitions. First, spontaneous recombination of an electron in the conduction band and a hole in the valence band, which leads to incoherent emission. Second, photon absorption by the active material, which creates electron-hole pairs and increases carrier densities in the conduction and valence bands. Third, photon emission from electron-hole recombination after photon excitation, which leads to optical gain. The dynamics of carrier and photon densities are controlled by coupled rate equations, which describe how electrons and holes are converted into photons. Photon emission processes contribute to increasing the photon density, while photon absorption and optical losses lead to a reduction in photon density.

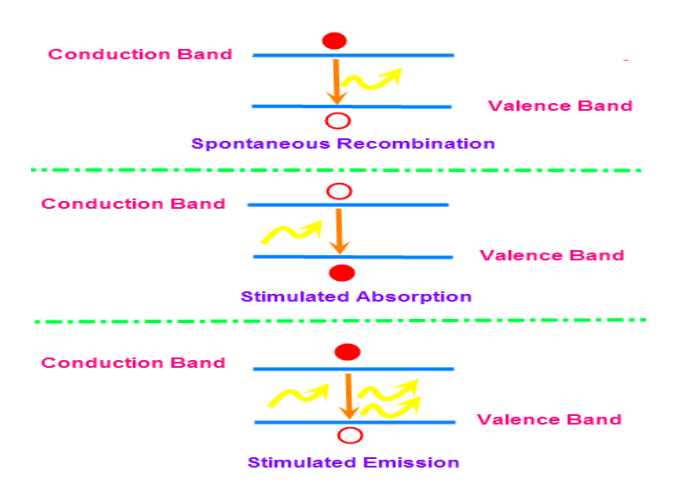


Figure 11: Electron transitions in a semiconductor material.

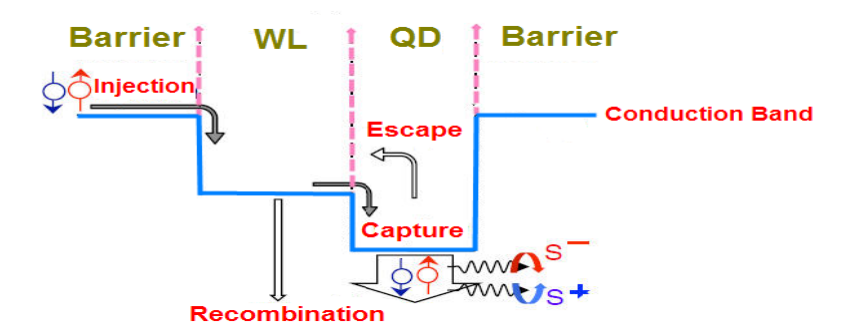


Figure 12: Characteristic Processes in Spin-Polarized Quantum Dot Semiconductor Laser

In quantum dot semiconductor lasers, the wetting layer (WL) serves as a carrier reservoir and significantly influences the device's dynamic behavior. This wetting layer, formed as a result of the self-assembly growth process, is an unavoidable feature in such devices. Quantum dot semiconductor lasers require lower currents to reach the threshold and sustain operation, and ideally, the threshold current should not be temperature-sensitive. After being injected into the wetting layer, electrons remain confined there for a period before relaxing into the quantum dots. Additionally, electrons in the wetting layer can recombine with holes or undergo stimulated emission to produce photons. Electrons that escape from the quantum dots do not contribute to the laser's efficiency and effectively become confined in the wetting layer. The rate equations for quantum dot semiconductor lasers are derived based on the occupation probabilities of energy states by electrons in the quantum dots and wetting layer, as well as photon occupation. These rate equations, expressed in terms of the occupation probabilities of electrons in the wetting layer f_w the quantum dots f_{qn} and photon populations f_s are formulated as follows:

$$\frac{df_{w}}{dt} = J(1 - f_{w}) - \frac{f_{w}(1 - f_{qn})}{\tau_{c}} + \frac{2f_{qn}(1 - f_{w})}{k\tau_{e}}$$
(1)

$$\frac{df_{qn}}{dt} = \frac{kf_w(1 - f_{qn})}{2\tau_c} - \frac{f_{qn}(1 - f_w)}{\tau_e} - b_q f_{qn}^2 - g(2f_{qn} - 1)f_s)$$
(2)

$$\frac{df_s}{dt} = g(2f_{qn} - 1)f_s - \frac{f_s}{\tau_{ph}}\tag{3}$$

Where $_J$ τ_{ph} , b_q , k, τ_e , τ_c and g represent, respectively: the number of electrons injected into the laser per unit time in each state of the wetting layer, the electron capture time, the electron escape time, the ratio of the number of states in the wetting layer to the number of quantum dots, the recombination rate in the quantum dots, the photon lifetime, and the stimulated emission rate. In Equation (3), the spontaneous emission factor and the optical confinement factor are set to 0 and 1, respectively.

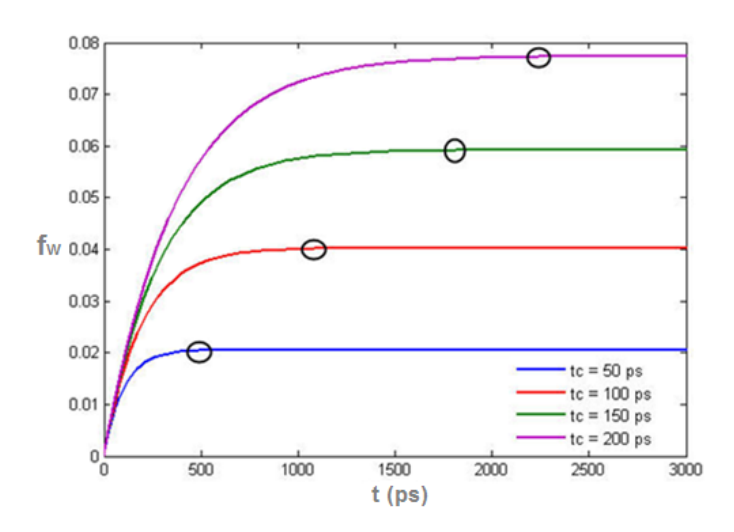


Figure 13: Temporal Dependence of the Occupation Probability of Wetting Layer States by Electrons in a Quantum Dot Semiconductor Laser

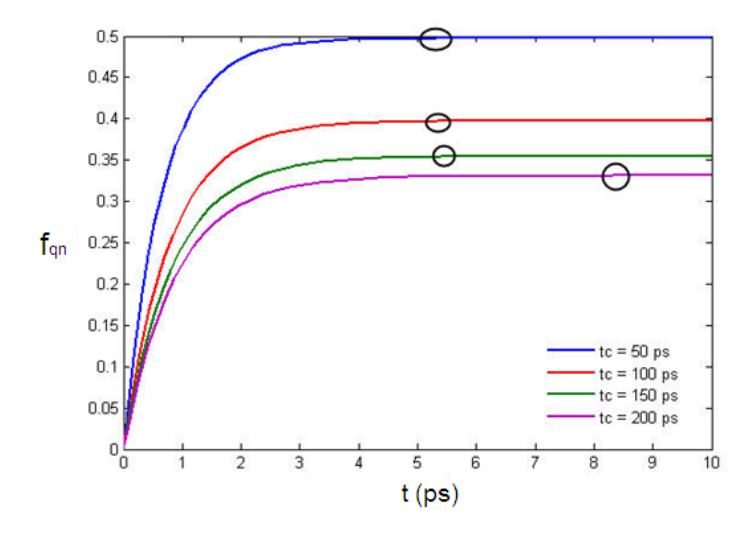


Figure 14: Temporal Dependence of the Occupation Probability of Quantum Dot States by Electrons in a Quantum Dot Semiconductor Laser

Based on these figures, the occupation probability of the wetting layer states by electrons increases with the electron capture time, while the occupation probability of quantum dot states by electrons increases as the electron capture time decreases under constant injection. When electrons are directly injected into the wetting layer, shorter electron capture times result in faster confinement of electrons in the quantum dots, leading to an increase in the occupation probability of quantum dot states by electrons. The points marked with black circles indicate that beyond a certain point, the occupation probabilities of quantum dot and wetting layer states reach a steady state and saturate. The obtained values for the occupation probabilities of wetting layer and quantum dot states for three different electron capture times are shown in:

Table 1: Obtained values of occupation probabilities of wetting layer states for three different electron capture times.

$\tau_c = 50 ps$		$\tau_c = 100 ps$		$\tau_c = 150 ps$	
f_w	t(ps)	f_w	t(ps)	f_w	t(ps)
0.0125	91.7065	0.0207	137.8592	0.0418	344.1086
0.0197	308.7805	0.0389	638.1196	0.0564	850.4725
0.0205	527.0261	0.0402	1155.8	0.0592	1814.9

Table 2: Obtained values of occupation probabilities of quantum dot states for three different electron capture times.

$\tau_c = 50 ps$		$\tau_c = 100 ps$		$\tau_c = 150 ps$	
f_{qn}	t(ps)	f_{qn}	t(ps)	f_{qn}	t(ps)
0.1346	0.2093	0.1297	0.3139	0.1268	0.3767
0.4928	3.1134	0.3943	3.8449	0.3520	4.1493
0.4972	5.3287	0.3970	5.3449	0.3542	5.6493

According to Figure 15, photon occupation increases with the rise in the occupation probability of quantum dot states under constant injection. As the occupation probability of quantum dot states by electrons increases, the number of electrons participating in the lasing process grows. Consequently, this increase enhances the coupling efficiency between carriers and light. This condition promotes stimulated emission, improving laser operation.

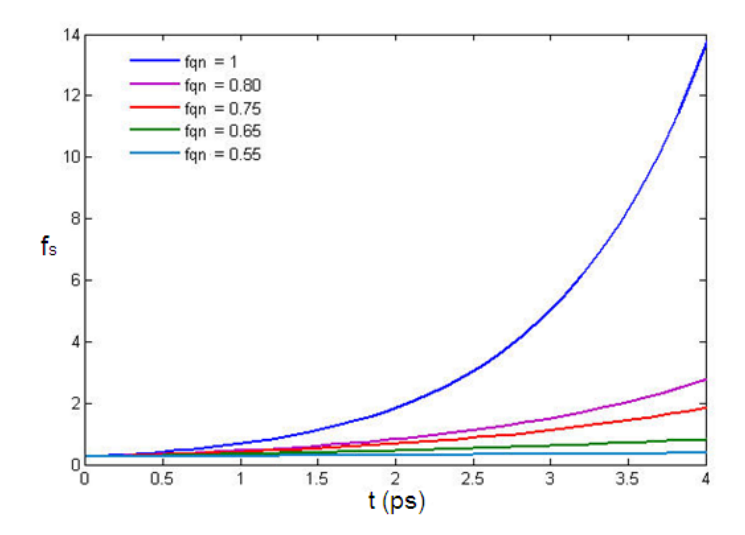


Figure 15: Temporal Dependence of Photon State Occupation in a Quantum Dot Semiconductor Laser.

Table 3: Obtained values of photon occupation for three different levels of quantum dot state occupation probability.

$f_{qn} = 0.70$		$f_{qn} = 0.73$		$f_{qn} = 0.75$	
f_s	t(ps)	f_s	t(ps)	f_s	t(ps)
0.1568	2.2500	0.2377	2.2788	0.3869	2.7059
0.2858	5.2500	0.7433	5.2788	1.5283	5.4534
0.6360	9.2500	3.3986	9.2788	11.4725	9.4845

By generalizing the rate equations, the occupation probabilities for spin-polarized electrons in the quantum dot and wetting layer states $(f_{w\pm},f_{qn\pm})$ and spin-dependent photon state occupation probabilities $(f_{S\mp})$ for a spin-polarized quantum dot semiconductor laser can be expressed as follows:

$$\frac{df_{w\pm}}{dt} = J_{n\pm}(1 - f_{w\pm}) - \frac{f_{w\pm}(1 - f_{qn\pm})}{\tau_c} + \frac{2f_{qn\pm}(1 - f_{w\pm})}{k\tau_e} \mp \frac{(f_{w+} - f_{w-})}{\tau_{snw}}$$
(4)

$$\frac{df_{qn\pm}}{dt} = \frac{kf_{w\pm}(1 - f_{qn\pm})}{2\tau_c} - \frac{f_{qn\pm}(1 - f_{w\pm})}{\tau_c} - b_q f_{qn\pm}^2$$
(5)

$$\frac{df_{S\mp}}{dt} = \Gamma_{QD}g(f_{qn\pm} + f_{qp\pm} - 1)f_{S\mp} - \frac{f_{S\mp}}{\tau_{ph}}$$

$$\tag{6}$$

Where $J_{n\pm}$ represent the number of spin-polarized electrons injected per unit time into the wetting layer for each spin state. The spin relaxation times in the wetting layer and quantum dots are denoted by τ_{snw} , τ_{snq} respectively, both of which are assumed to approach infinity. We neglect spin-dependent spontaneous radiative recombination in the wetting layer. Additionally, due to charge neutrality, the rate equations for spin-polarized electrons can be decoupled from those describing holes.

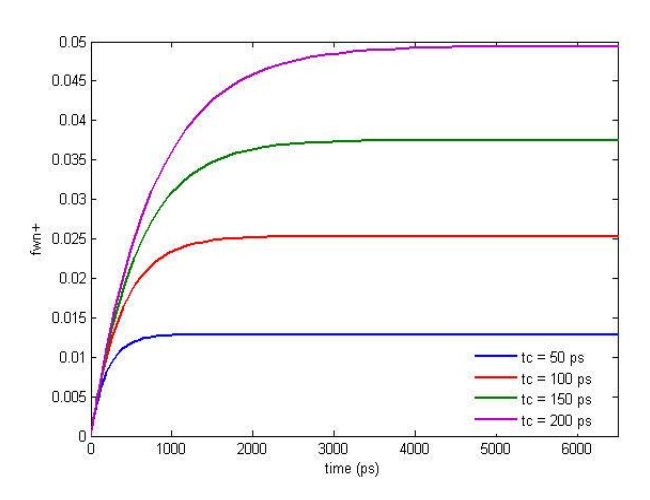


Figure 16: Temporal Dependence of the Occupation Probability of Wetting Layer States by Spin-High Electrons in a Spin-Polarized Quantum Dot Semiconductor Laser.

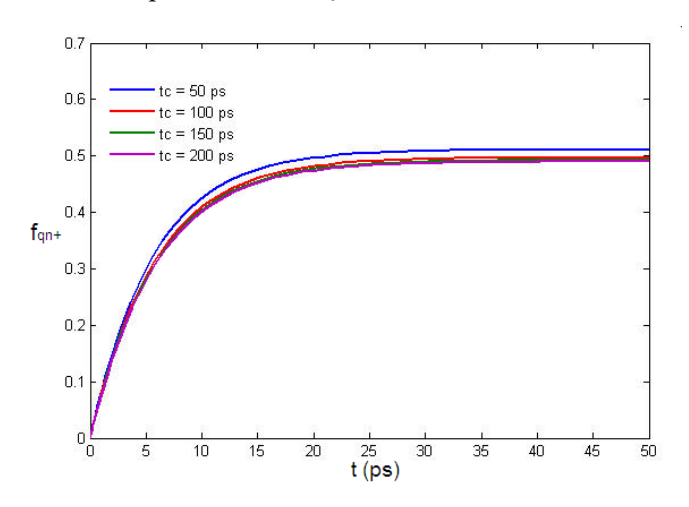


Figure 17: Temporal Dependence of the Occupation Probability of Quantum Dot States by Spin-High Electrons in a Spin-Polarized Quantum Dot Semiconductor Laser.

These figures show that as the electron capture time increases, the occupation probability of wetting layer states by spin-up electrons increases. Meanwhile, the occupation probability of quantum dot states by spin-up electrons increases with a decrease in the electron capture time under constant spin-polarized injection. The shorter the electron capture time, the faster the spin-up electrons become confined in the quantum dots, leading to an increase in the occupation probability of these states by the electrons. This process eventually reaches saturation.

Table 4: Obtained values of the occupation probability of wetting layer states by spin-up electrons for three different electron capture times.

$\tau_c = 50 ps$		$\tau_c = 100 ps$,	$\tau_c = 150 ps$	
f_{w+}	t(ps)	f_{w+}	t(ps)	f_{w+}	t(ps)
0.0096	270.3789	0.0164	407.3349	0.0226	530.2278
0.0111	390.3743	0.0203	626.3705	0.0288	844. 1998
0.0128	1009.3	0.0253	2333.1	0.0375	3688.1

Table 5: Obtained values of the occupation probability of quantum dot states by spin-up electrons for three different electron capture times.

$\tau_c = 50 ps$		$\tau_c = 100 ps$		$\tau_c = 150 ps$	
f_{qn+}	t(ps)	f_{qn+}	t(ps)	f_{qn+}	t(ps)
0.3500	6.4821	0.3425	6.7467	0.2736	4.7492
0.4964	19.7447	0.4823	20.1163	0.4739	18.9973
0.5099	33.4947	0.4959	33.8663	0.4917	37.7473

According to Figure 18, the occupation of photons with negative helicity increases with the occupation probability of spin-up quantum dot states under constant spin-polarized injection. As the occupation probability of spin-up quantum dot states increases, the number of spin-up electrons participating in the lasing process also increases. This results in enhanced carrier-light coupling efficiency, which describes the increase in the coupling between carriers and light. Consequently, this condition promotes stimulated emission and improves laser operation.

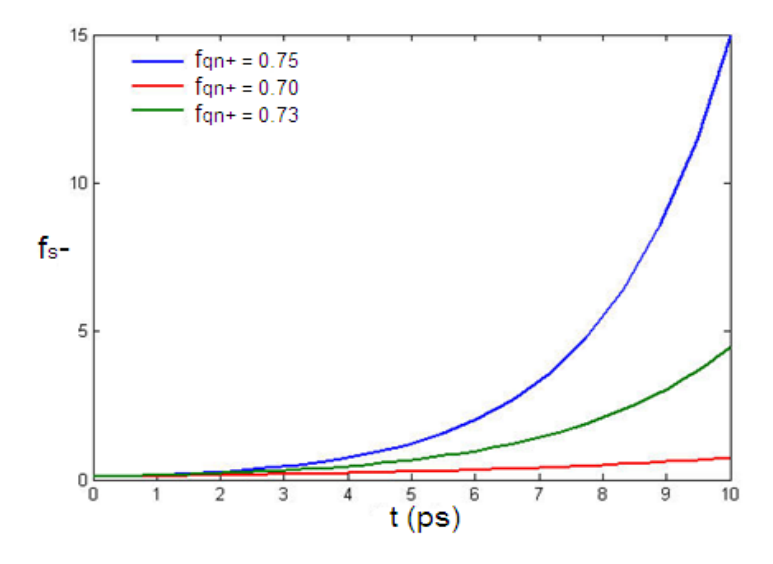


Figure 18: Temporal Dependence of Photon Occupation with Negative Helicity in Spin-Polarized Quantum Dot Semiconductor Lasers.

Table 6: Obtained values of photon occupation with negative helicity for the occupation probability of three different quantum dot states by spin-up electrons

$f_{qn+} = 0.$	70	$f_{qn+} = 0.73$		$f_{qn+} = 0.75$	
f_{s^-}	t(ps)	f_{s^-}	t(ps)	f_{s^-}	t(ps)
0.1051	0.2500	0.1105	0.2644	0.1163	0.3014
0.1568	2.2500	0.2377	2.2788	0.3869	2.7059
0.2858	5.2500	0.7433	5.2788	1.5283	5.4534

Normalized Spin Filtering Window Width:

The creation of a normalized spin filtering window is one of the important consequences of spin-polarized injection. The width of this window can be expressed as follows:

$$d = \left[\frac{1}{(1 - |P_{Jn}|)} \right] - \left[\frac{4}{(2 + |P_{Jn}|)^2} \times \left[1 + \frac{18|P_{Jn}^3|b_q\tau_c}{1 + 6|P_{Jn}| + 3|P_{Jn}^2| - 10|P_{Jn}^3|} \right] \right]$$
(7)

Where P_{in} is the polarization of the injected electron current.

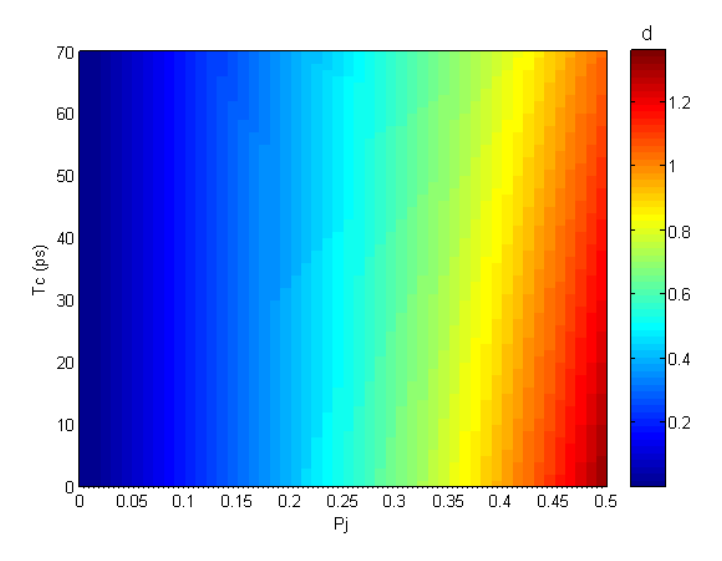


Figure 19: Variation of the normalized spin filtering window width as a function of injected electron current polarization and electron capture time.

In this figure, the dark red and blue regions represent the maximum and minimum values of the normalized spin filtering window width, respectively. From this, it is evident that the width of the normalized spin filtering window increases with a decrease in electron capture time and a simultaneous increase in the polarization of the injected electron current. An increase in the width of the normalized spin filtering window leads to a reduction in laser energy consumption and an

improvement in laser dynamic performance. This advantage is achieved through the use of spin-polarized electron injection in quantum dot/quantum well semiconductor spin-polarized lasers.

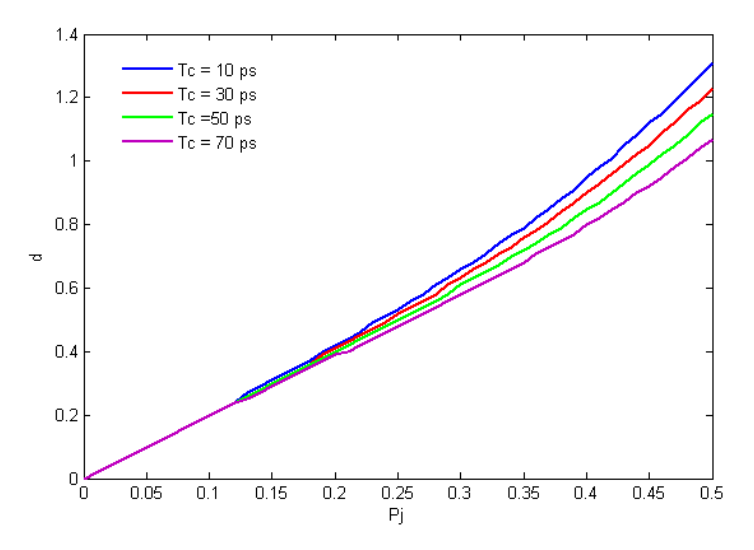


Figure 20: Variation of the normalized spin filtering window width as a function of the injected electron current polarization for four different electron capture times.

This figure shows that the normalized spin filtering window width increases with the increase in injected electron current polarization at each specific electron capture time. As the electron capture time increases, it takes longer for the electrons to fall into the quantum dot. Therefore, we observe a lower probability of spin-up electrons occupying smaller energy levels in the quantum dots, which results in a decrease in the normalized spin filtering window width.

Table 7: Values of the normalized spin filtering window width for three different injected electron current polarizations at various electron capture times.

$ P_{Jn} $ =	$ =0.2$ $ P_{Jn} =0.3$		0.3	$ P_{Jn} =0.4$	
d	$t_c(ps)$	d	$t_c(ps)$	d	$t_c(ps)$
0.41	30	0.63	30	0.90	30
0.40	50	0.61	50	0.85	50
0.39	70	0.58	70	0.80	70

Reduction of Threshold Current Density:

One of the advantages of spin-polarized injection is the reduction in threshold current density, which results from the creation of the normalized spin filtering window. In this window, only majority-spin charge carriers contribute to the lasing process. The reduction in threshold current density can be expressed as follows:

$$r = 1 - \frac{4}{\left(2 + |P_{Jn}|\right)^2} \times \left[1 + \frac{18|P_{Jn}^3|b_q\tau_c}{1 + 6|P_{Jn}| + 3|P_{Jn}^2| - 10|P_{Jn}^3|}\right]$$
(8)

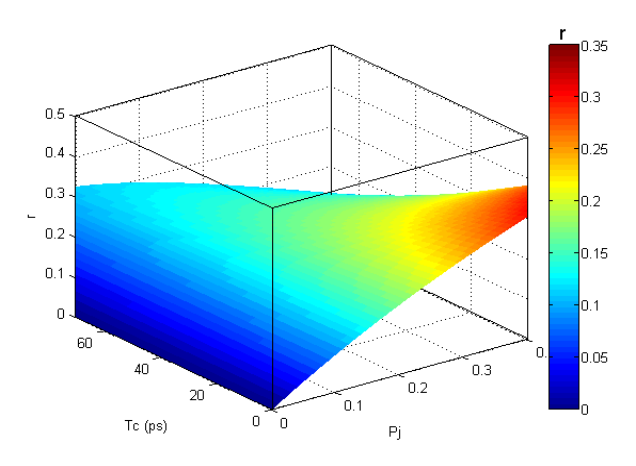


Figure 21: Three-Dimensional Variation of Threshold Current Density Reduction as a Function of Injected Electron Current Polarization and Electron Capture Time.

According to the figure, it can be observed that the reduction in threshold current density increases with a simultaneous decrease in electron capture time and an increase in the injected electron current polarization. Additionally, the increase in threshold current density reduction results in lower laser energy consumption and improved laser dynamic performance. Such a reduction is achieved through the use of spin-polarized electron injection in quantum well spin-polarized semiconductor lasers. An increase in spin-polarized electron injection leads to an increase in injected electron current polarization and laser bandwidth. It should be noted that the reduction in threshold current density increases with the increase in injected electron current polarization at each specific electron capture time. As the electron capture time increases, we observe smaller values of the normalized spin filtering window width and a reduction in threshold current density.

Table 8: Values of threshold current density reduction for three different injected electron current polarizations at various electron capture times.

$ P_{Jn} =0.1$		$ P_{Jn} =0.2$		$ P_{Jn} =0.4$	
r	$t_c(ps)$	r	$t_c(ps)$	r	$t_c(ps)$
0.089	30	0.174	30	0.353	30
0.087	50	0.168	50	0.341	50
0.085	70	0.163	70	0.328	70

Optical Gain:

Optical gain describes the coupling efficiency between carriers and light, which leads to stimulated emission. The spin-dependent optical gain can be written as follows:

$$G_{\pm} = g(f_{qn\pm} + f_{qp\pm} - 1)f_{S\mp} \tag{9}$$

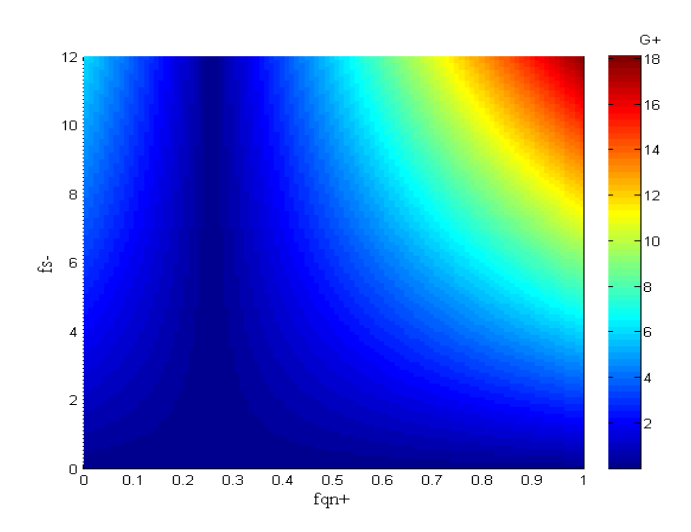


Figure 22: Spin-High Optical Gain as a Function of the Occupation Probability of Spin-High Electron States and Photon Occupancy with Negative Helicity in Quantum Dots.

The occupation probability of higher states by spin-up electrons in the quantum dot leads to the occupation of photons with high negative helicity. As a result, we obtain higher values for the spin-up optical gain. The increase in spin-up optical gain ensures the laser's efficiency.

Table 9: Obtained values of spin-up optical gain for four different levels related to the occupation probability of electrons in quantum dots.

$f_{qn+} =$	1	$f_{qn+} = 0.80$		$f_{qn+} = 0.75$		$f_{qn+} = 0.55$	
f_{s^-}	$G_{\scriptscriptstyle +}$	f_{s^-}	$G_{\scriptscriptstyle +}$	f_{s^-}	$G_{\scriptscriptstyle +}$	f_{s^-}	$G_{\scriptscriptstyle +}$
3.5	5.40	3.5	3.96	3.5	3.60	3.5	2.16
8.2	12.45	8.2	9.13	8.2	8.30	8.2	4.98
11.7	17.70	11.7	12.98	11.7	11.80	11.7	7.08

Chapter 5: Conclusion

Conclusion:

Based on the calculations and analyses conducted in this thesis, the performance of spin-polarized quantum dot semiconductor lasers is highly dependent on spin injection and longer spin relaxation times. By numerically solving the rate equations, we investigated the simultaneous effects of electron capture time and injected current polarization on the reduction of threshold current density and the normalized spin filtering window width. The results showed that both the reduction in threshold current density and the normalized spin filtering window width increase with a decrease in electron capture time and an increase in injected current polarization. This increase leads to a reduction in energy consumption and an improvement in the dynamic performance of the laser. The maximum reduction in threshold current density and the normalized spin filtering window width were found to be 0.353 and 0.90, respectively. Additionally, the spin-up optical gain increased with the probability of occupation of higher states by spin-up electrons, reaching a maximum value of 17.70. This research could contribute to new advancements in the field of

colloidal II-VI quantum dot semiconductor lasers, such as CdS, CdSe, ZnSe, and ZnTe, and provide insights into spin transport and magnetism in these devices.

References:

- 1. Kovalenko, M. V. et al. Prospects of nanoscience with nanocrystals. ACS Nano 9, 1012–1057 (2015).
- 2. Kagan, C. R., Lifshitz, E., Sargent, E. H. & Talapin, D. V. Building devices from colloidal quantum dots. Science 353, pii: aac5523 (2016).
- 3. Pietryga, M. et al. Spectroscopic and device aspects of nanocrystal quantum dots. Chem. Rev. 116, 10513–10622 (2016).
- 4. Klimov, V. I. et al. Optical gain and stimulated emission in nanocrystal quan-tum dots. Science 290, 314–317 (2000).
- 5. Hu, J. et al. Flexible integrated photonics: where materials, mechanics and optics meet. Opt. Mater. Express 3, 3989–3994 (2013).
- 6. Ozcelik, D. et al. Optofluidic bioanalysis: fundamentals and applications. Nanophotonics 6, 647–661 (2017).
- 7. Bisschop, S., Geiregat, P., Aubert, T. & Hens, Z. The impact of core/shell sizes on the optical gain characteristics of CdSe/CdS quantum dots. ACS Nano 12,9011–9021 (2018).
- 8. Klimov, V. Optical nonlinearities and ultrafast carrier dynamics in semi-conductor nanocrystals. Phys. Chem. B 104, 6112–6123 (2000).
- 9. Xie, W. et al. Colloidal quantum dots enabling coherent light sources for integrated siliconnitride photonics. J. Sel. Top. Quant. Electr. 23, 1–13 (2017).
- 10. García-Santamaría, F. et al. Suppressed Auger recombination in 'giant' nano-crystals boosts optical gain performance. Nano Lett. 9, 3482–3488 (2009).
- 11. Park, Y.-S., Bae, W. K., Baker, T., Lim, J. & Klimov, V. I. Effect of auger recombination on lasing in heterostructured quantum dots with engineered core/shell interfaces. Nano Lett. 15, 7319–7328 (2015).
- 12. Lim, J., Park, Y.-S. & Klimov, V. I. Optical gain in colloidal quantum dots achieved with direct-current electrical pumping. Nat. Mater. 1–41 (2017).
- 13. Fan, F. et al. Continuous-wave lasing in colloidal quantum dot solids enabled by facet-selective epitaxy. Nature 544, 75–79 (2017).
- 14. Adachi, M. M. et al. Microsecond-sustained lasing from colloidal quantum dot solids. Nat. Commun. 6, 8694 (2015).
- 15. Fan, F. et al. Continuous-wave lasing in colloical quantum dot solids enabled by facet-selective epitaxy. Nature 544, 75–79 (2017).
- 16. Lim, J., Park, Y.-S. & Klimov, V. I. Optical gain in colloidal quantum dots achieved with direct-current electrical pumping. Nat. Mater. 17, 42–49 (2017).
- 17. Xie, W. et al. On-Chip Integrated Quantum-Dot Silicon-Nitride Microdisk Lasers.Adv. Mater. 29, 1604866 (2017).